

Title: Toolbox for the structure-guided evolution of ferulic acid decarboxylase (FDC)

Author list: Horia Duță[†], Dr. Alina Filip[†], Dr. Levente Csaba Nagy, Dr. Emma Zsófia Aletta Nagy, Dr. Róbert Tóth, Dr. László Csaba Bencze^{*}

Affiliation: Enzymology and Applied Biocatalysis Research Center, Faculty of Chemistry and Chemical Engineering, Babeş-Bolyai University, Arany János street 11, RO-400028 Cluj-Napoca, Romania

^{*} Address for correspondence: Dr. László Csaba Bencze; e-mail: cslbencze@chem.ubbcluj.ro

[†] These authors contributed equally to this work

ABSTRACT

The interest towards ferulic acid decarboxylase (FDC), piqued by the enzyme's unique 1,3-dipolar cycloaddition mechanism and its atypic prFMN cofactor, provided several applications of the FDC mediated decarboxylations, such as the synthesis of styrenes, or its diverse derivatives, including 1,3-butadiene and the enzymatic activation of C-H bonds through the reverse carboligation reactions. While rational design-based protein engineering was successfully employed for tailoring FDC towards diverse substrates of interest, the lack of high-throughput FDC-activity assay hinders its directed evolution-based protein engineering. Herein we report a toolbox, useful for the directed evolution based and/or structure-guided protein engineering of FDC, which was validated representatively on the well described FDC, originary from *Saccharomyces cerevisiae* (*ScFDC*). Accordingly, the developed fluorescent plate-assay allows in premiere the FDC-activity screens of a mutant library in a high-throughput manner. Moreover, using the plate-assay for the activity screens of a rationally designed 23-membered *ScFDC* variant library against a substrate panel comprising of 16, diversely substituted cinnamic acids, revealed several variants of improved activity. The superior catalytic properties of the hits revealed by the plate-assay, were also supported by the conversion values from their analytical scale biotransformations. The computational results further endorsed the experimental findings, showing inactive binding poses of several non-transformed substrate analogues within the active site of the *wild-type ScFDC*, but favorable ones within the catalytic site of the variants of improved activity. The results highlight several 'hot-spot' residues involved in substrate specificity modulation of FDC, such as I189, I330, F397, I398 or Q192, of which mutations to sterically less demanding residues increased the volume of the active site, thus facilitated proper binding and increased conversions of diverse non-natural substrates. Upon revealing which mutations improve the FDC activity towards specific substrate analogues, we also provide key for the rational substrate-tailoring of FDC.

1. INTRODUCTION

Ferulic acid decarboxylase (FDC), as member of the carboxy-lyase family (EC 4.1.1.) has attracted significant interest in recent years, mainly due to its unusual, prenylated flavin mononucleotide (prFMN) cofactor¹, as well as to its unique mechanism, representing the first enzymatic 1,3-dipolar cycloaddition^{2,3}. Besides the studies focusing on the elucidation of the structure and mechanism of FDC, as first application of FDC, the biosynthesis of styrene, involving the decarboxylation of cinnamic acid within engineered *E.coli* cells, has been

reported^{4,5}. Subsequently, FDC was shown to possess broad substrate tolerance, decarboxylating differently (*ortho*-, *meta*- or *para*-) substituted cinnamic acids, as well as its biaryl or heteroaryl derivatives^{2,6,7}. Recently, FDC has been employed in an enzymatic cascade yielding stilbenes⁸ or shown to activate C-H bonds through CO₂ fixation, yielding unsaturated aromatic carboxylic acids⁹. Other studies investigated the effect of mutations/deletions of *fdc1* on the production of volatile phenols obtained during yeast alcoholic fermentation¹⁰, or quantitatively monitored the fermentation byproducts when *fdc1* in *S. cerevisiae* and *S. eubazanus* have been CRISPR edited¹¹. The effect of *fdc1* single nucleotide polymorphisms (SNPs) on the decarboxylation activity of some industrially relevant yeasts was also reported¹².

The stability issues of the prFMN cofactor¹³, as one the major factors limiting the applicability of FDC reactions, can be alleviated by the use of whole-cells^{6,7,14} or cell-free extracts¹⁵ FDC-biocatalysts. Recently, several studies focused on the biosynthesis of the cofactor, aiming it's *in vivo* or *in vitro* synthesis¹⁶, that provides access to the fully active, holo-FDC. In *Saccharomyces cerevisiae*, the final step in the cofactor's biosynthesis, the prenylation of FMN, is catalyzed by PAD1, a flavoprotein that is necessary for the generation of active, holo-FDC. In *E. coli*, UbiX substitutes PAD1 in its role of prFMN's biosynthesis, that serves as cofactor for UbiD, homologue of FDC¹⁷. As such, needing both *fdc1* and *pad1* genes for the desired decarboxylase activity¹⁸, initially FDC has been studied in *S. cerevisiae* cultures, while later it has been shown that *E. coli* cultures expressing only the *fdc1* gene, due to the presence of UbiX of the host *E. coli* cells, can also function as whole-cell biocatalysts with the desired FDC-activity^{7,17-20}. Supposedly, the cofactor's active iminium form is obtained inside FDC's active site under the influence of oxygen²¹ and a number of conserved residues²². However, in solution, prFMNH₂ can be irreversibly converted to inactive forms, such as prFMN C_{4a}-OOH²¹, prFMN-OH, prFMN_{radical}, prFMN_{radical}-H, prFMN_{iminium}-OH, C₁-ene-prFMN_{iminium}^{1,13,23,24}, while light decomposure has been also reported²², all these hindering the isolation of the holo-FDC.

Despite the cofactor stability issues, the identification of several novel decarboxylases harboring the prFMN cofactor²⁵⁻²⁸, the broad substrate scope of FDC in comparison to phenolic acid decarboxylases from *Enterobacter sp.* or *Bacillus pumilus*²⁹⁻³¹, or to benzoic acid decarboxylases³², that are limited to decarboxylations of 4-OH cinnamates, or of benzoic acids, respectively, propelled FDC as one of the most versatile non-oxidative decarboxylases. Moreover, the high-quality crystal structures of FDC in apo-, holo- and ligand bound variants^{1,33-35} and the elucidation of the 1,3-cycladdition reaction mechanism¹⁻³, allowed initial rational design of FDC towards different substrates of interest, such as aromatic carboxylic acids, bulky cinnamic acid analogues and/or aliphatic substrates^{7,9,36}.

Encouraged by the versatility of FDC and its increasing biotechnological applicability, herein we provide a toolbox for the efficient laboratory evolution of FDC. Accordingly, we describe the development of a facile, fluorescent cell-plate FDC-activity assay, validated by its employment within the activity screens of a focused FDC mutant library towards a substrate panel of high structural diversity. The increased activities of the FDC variants selected from the plate-assay, were confirmed by performing analytical scale biotransformations. Computational results supported and revealed the molecular level details of the improved enzyme activities. Notable, that despite the results represent an initial snapshot of employing the developed laboratory evolution toolbox for FDC, the obtained correlation between the nature/position of a certain functional group of the substrate and the corresponding mutations of active site residues providing improved decarboxylation activity, also paves the way for the substrate-tailored protein engineering of FDC.

2. RESULTS AND DISCUSSION

2.1. Generation of substrate panel and focused FDC mutant library

Initially, we generated a focused *Sc*FDC mutant library (Table S1), by the individual replacement of active site residues to smaller alanine or valine residues (Fig. 1) in order to alleviate the steric repulsion of the targeted substrate panel (Fig. 2), predicted by the docking studies using our computational model⁷. Among the substrate panel we included substrate analogues with ring-substituents of diverse electronic properties (**1a-1e**), or multiple substituted in various, *o*-, *m*-, *p*- positions of the aromatic ring (**1f-1i**), as well as heteroaromatic (**1j**, **1k**), or differently connected bulky, biaryl (**1l-1o**) or heteroaryl (**1p**) substrate analogues, of which active site orientations in several cases showed steric repulsions with active site residues of *Sc*FDC. Notable, that compound **1p** of the substrate panel was not transformed by *wild-type* FDC⁷, while for bulky biaryl compounds (**1l-1o**) no proper active site orientations were obtained by the initial docking predictions.

The selected active site residues involve Q192 and I330, previously found to narrow the active site of *Sc*FDC, forming a gate, which hinders the accommodation of bulky non-linear substrates⁷. Since Q192 is also involved in cofactor binding through hydrogen bonding with the ribitol tail of prFMN (Figure S23), besides mutation Q192A, variant Q192N was also considered. During the experimental work of our study, other studies implying protein engineering of *An*FDC and *Sc*FDC has been reported, involving several active site residues F397, I398, M286 and I330, also selected by us for the mutant library generation. Accordingly, mutation of residues Y394, T395 of *An*FDC and the corresponding homologue residues F397 and I398 of *Sc*FDC provided FDC variants with decarboxylase activity for 1,3-cyclobutadiene³⁶. Site-saturation mutagenesis at residues M283 and I327 of *An*FDC (corresponding to M286 and I330 in *Sc*FDC) provided FDC mutants with activity within the decarboxylation of atypic, benzoic acid-type aromatic substrates⁹. Besides these residues, our molecular docking predicted I189 as narrowing the catalytic site, providing steric repulsion in case of substrates with multiple substituted aromatic moieties, while replacement of bulky F440 residue in combination with L442 into smaller hydrophobic residues, was also considered. Notable, that all selected *Sc*FDC active site residues, except F397 and I398 (corresponding to Y394 and T395 of *An*FDC) are conserved within the two highly studied *Sc*FDC and *An*FDC variants (Table S2).

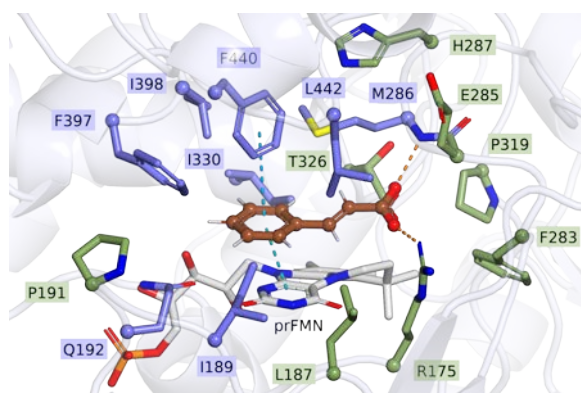


Fig. 1. Active site model of *Sc*FDC (PDB: 4ZAC) with *trans*-cinnamic acid as substrate analogue, highlighting in green the residues selected for individual replacement with alanine/valine.

2.2 Cell-plate assay development

While the protein engineering of FDC is of high interest, for an efficient directed evolution-based engineering process, high-throughput activity assays, allowing facile activity screens of largely sized mutant libraries, are highly desirable. A plate assay, suitable for FDC activity screens at whole-cell level, also alleviates the tedious isolation process of holo-FDC^{1,20}, however according to our knowledge, no such activity assay has been reported for FDC. Recently, we reported a fluorescent phenylalanine ammonia-lyase (PAL) activity assay, that employs FDC as secondary, reporter enzyme, the produced styrene being fluorescently detected upon its reaction with a tetrazole-based fluorogenic probe³⁷. While the PAL-activity assay performed optimal using cell-free extracts³⁷. herein we focused on adapting the fluorescent detection of styrene derivatives to a cell-plate FDC-activity assay. The 1,3-dipolar cycloaddition reaction between an alkene and a tetrazole represents an attractive method of fluorophore-forming bioorthogonal chemistry, with various diaryltetrazoles shown to be highly sensitive fluorophores for the detection of alkenes³⁸⁻⁴⁰. Furthermore, the photoinduced 1,3-dipolar cycloaddition using the selected diaryltetrazole (Fig. 2) as nitrile imine dipole was previously shown to possess compatibility for *in vivo* protein labeling within *E. coli* whole cells³⁹⁻⁴¹.

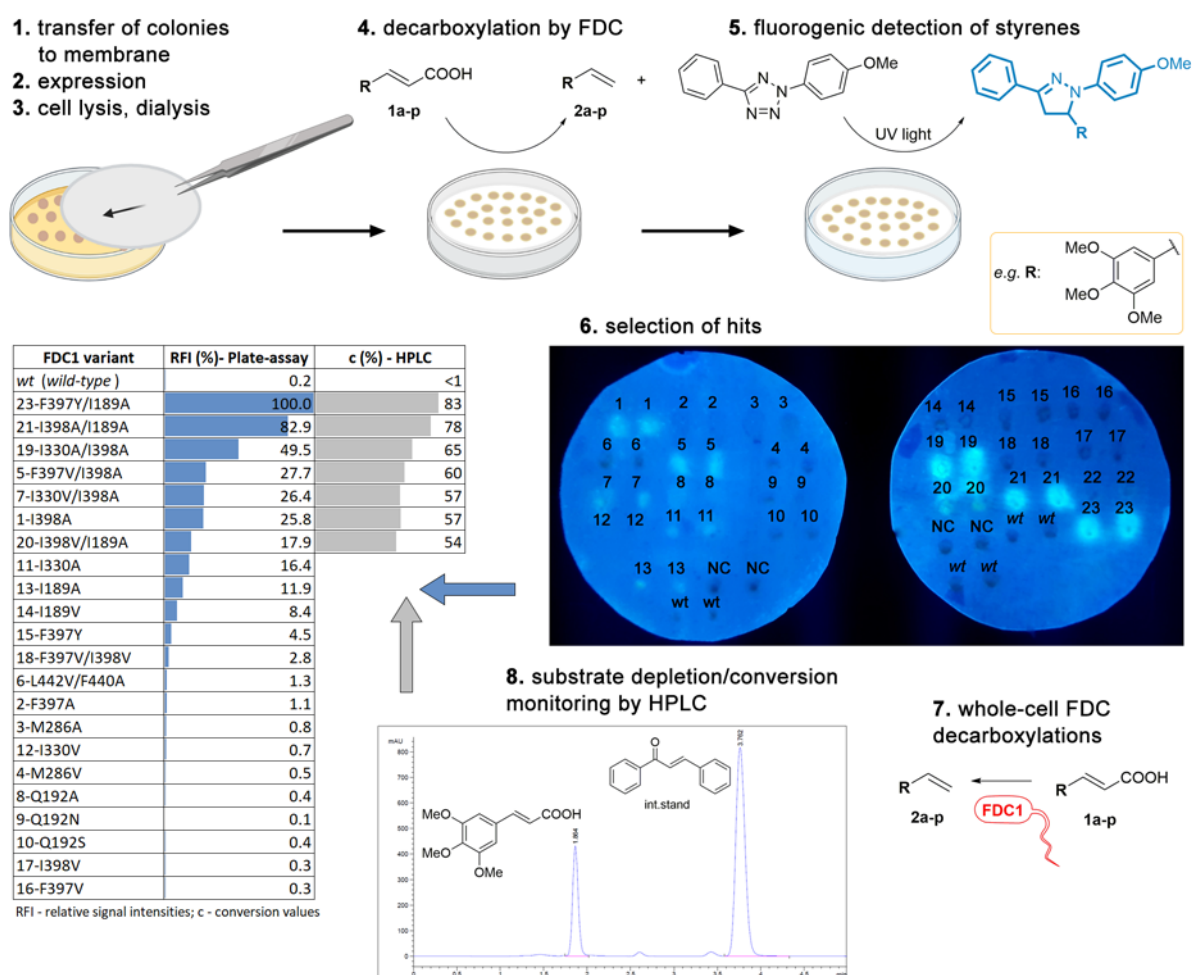


Fig. 2. Initial FDC activity screens using the fluorescent cell-plate assay allowing rapid identification of enzyme variants with improved activity, that has been also confirmed by the increased conversion values determined from the whole-cell biotransformations. Representative results are presented in case of substrate analogue 3,4,5-trimethoxy-cinnamic acid **1i** (for details of image preparations see *Supplementary Information*, Chapter 6).

Accordingly, within the cell-plate assay whole cells harboring the *fdc1* gene variants of our mutant library were tested as biocatalyst in the decarboxylation reactions of the entire substrate panel. During this initial activity screens, cell plates with the colonies harboring the FDC variants (in duplicates) and a negative control, *E. coli* host cells without the plasmid containing *fdc1* gene, were grown, transferred onto a PVDF membrane, followed by gene expression induced by IPTG (Fig. 2). Cell permeabilization with chloroform, and a subsequent dialysis step of the membrane-attached colonies was followed by the decarboxylation reactions, performed by placing the membrane onto the plate containing 2 mM of the corresponding substrates **1a-1p**, followed by incubation at 37 °C for 4 hours. For the subsequent fluorogenic reaction, incubation of the membrane with the tetrazole fluoroprobe and UV-irradiation was employed, followed by the detection of the fluorescence signal through an imaging system (Fig. 2).

2.3 FDC-activity screens

The developed cell-plate assay has been employed for the initial, qualitative assessment of the enzyme activities of the FDC mutant library towards the substrate panel. Allowing the selection/identification of the best performing variants, based on their relative fluorescence signal intensities (Fig. 2, Tables S3-S5). Furthermore, the selected variants, used as induced whole cell biocatalysts were used in analytical scale biotransformations of the corresponding substrates, monitoring the conversion values by reverse phase HPLC. The activity-order of the variants based on the fluorescent signal intensities from the cell-plate assay (Tables S3-S5) were in good correlation with the conversion-based activity ranking of the hits selected from mutant library (Fig. 3, Tables S7-S21). This correlation supports the applicability of the fluorescent plate-assay for qualitative FDC-activity assessments, useful for the initial high-throughput activity screens of directed evolution processes.

Besides, during the activity screens, several “hot-spot” active site residues, which upon mutations resulted FDC variants of improved activity, have been identified. Interestingly mutation of residue F397 of *ScFDC* to tyrosine, its homologue residue from *AnFDC*, in several cases, such as decarboxylations of **1c**, **1g**, **1l**, **1n** and **1o**, provided increased fluorescent signals and conversions. Notable the existence of other two differences in the active site residues of the two FDC variants (Table S2), with I398 of *ScFDC* having as homologue the more polar T395 of *AnFDC1*, while residue P319, located distal to the substrate’s aromatic substituent, is replaced by C316 in the *Aspergillus* variant. Mono-ethoxy substituted cinnamic acids **1a** and **1b**, transformed by *wild-type ScFDC* with moderate conversions (Fig. 2) of 63% and 71%, respectively, were quantitatively decarboxylated by variants I189A/V, suggesting a preferable orientation of the *ortho*-, *meta*- substituents towards residue I189. In case of *para*-substituted substrates **1c-1e**, mutation of residues F397 and I398 improved the enzyme activity, resulting in conversions up to 78% and 93%, respectively, in comparison with the 39% (for **1c**) and 22% (for **1d**) conversions provided by the *wild-type* enzyme. The sterically more demanding *tert*-butyl substituted derivative **1e** was not transformed either by *wild-type* or single mutants F397V or I398A(V) variants, however double mutant variants F397V/I398A and F397V/I398V provided conversions of 11% and 24%, revealing an additive effect of the combined mutations. The active site orientation of the substrate’s aromatic substituents, depicted by the biotransformations of mono-substituted derivatives, were also supported by the decarboxylations of the disubstituted substrates **1f-1h**. Notable, that substrate analogues **1f** and **1g**, disubstituted in the *meta*, *para*- position of the aromatic ring, resemble the substitution pattern of the natural substrate, ferulic acid. Thus, expectedly *wild-type ScFDC* transforms all three disubstituted substrates, obtaining high conversions of 66% in case of **1f**, and moderate/low conversions for the dimethoxy-cinnamic

acids (14% in case of **1g**, and 33% in case of **1h**). In accordance with previous reports^{2,7}, this result support that electronic effects also influence the enzyme activity of FDC. However, aiming to find residues, of which mutations lead to improved activities, we continued to focus on the relative activity increment within the variant library towards each individual substrate. Accordingly, the significant improvements in conversion values in case of 3,4-dimethoxycinnamic acid **1g** when using mutant variants I189A/V and I398A (increase with 45-52 % in comparison with *wild-type*), corresponds with the supposed orientation of the *meta*- and *para*-substituents towards residues I189 and I398, respectively. In case of 2,5-dimethoxycinnamic acid **1h**, besides the expected superior activity of I189A and I398A/I189A variants, reflected in an increase of conversion values with 29% and 33%, relative to those obtained with the *wild-type* FDC, variant I330A provided the highest activity increase ($c_{I330}=73\%$, while $c_{wt}=33\%$). This suggests, that in case when substituents occupy both *ortho*-, or *meta*-positions from the different sides of the aromatic ring, two active site residues, namely I189 at one side and I398/I330 on the other side of the active site, are involved in the substituents accommodation. The biotransformations of the 3,4,5-trimethoxy-cinnamic acid **1i** further supports this correlation, while *wild-type* FDC proved to be inactive, double mutant variants, such as I330A(V)/I398A, I398A(V)/I189A or F397V(Y)/I398A, including mutations of residues I398, F397 (for *para*-positioned substituents) or I189, I330 (for *meta*-substituents) provided superior variants, resulting in conversions of 54–83% (**Figure 2**, **Figure 3**, Table S15).

Definitely, substrate accommodation of bi(hetero)-aromatic substrate analogues **1j-1p** is less predictable based on the active site model (Fig. 1), therefore the mutation-activity increase correlation, revealed by the activity screens, is even more valuable for the structure-guided protein engineering of FDC. Despite that heteroaromatic, bicyclic derivatives **1j** and **1k** show a different structural architecture, with functionalization occurring in the 3' and 2' positions of the heteroaryl rings, similar mutations of residues I189, I330 provide variants I189A(V) and I330A, with superior conversions of ~90% (**1j**), 45–63% (**1k**) to the moderate conversions of 53% (**1j**) and 38% (**1k**) obtained by the *wild-type* FDC. Regarding the transformations of bulkier, differently connected biaryl substrate analogues **1l-1o**, *wild-type* ScFDC showed low (12% and 23% conversions for **1l** and **1m**, respectively) or no activity (**1n**, **1o**). Besides the expected beneficial effect of individual or combined mutations of F397A and I398A(V), providing superior variants with good to moderate conversions, mutant variant F397Y also resulted in improved 41.5% and 65.3% conversions for **1n** and **1o**, respectively. Generally, in case of these bulky substrates **1l-1o**, mutations of similar hot-spot residues (I189, Q192, F397, I398) provided single/double mutant variants of high activity, leading to conversions between 51–81% for compounds **1m-o**. In case of (*E*)-3-(10-methyl-10H-phenothiazin-3-yl)acrylic acid **1p**, the high background fluorescence, most probably provided by the phenothiazine moiety, hindered the cell-plate activity screens, while in the analytical scale biotransformations of **1p** none of the ScFDC variants of the mutant library provided detectable conversions.

Accordingly, the activity screens of the FDC variant library towards the substrate panel provided a comprehensive active site map, which correlates the substitution pattern of the substrate's aromatic moiety with their specific active site positioning, strengthening the rational design-based FDC engineering.

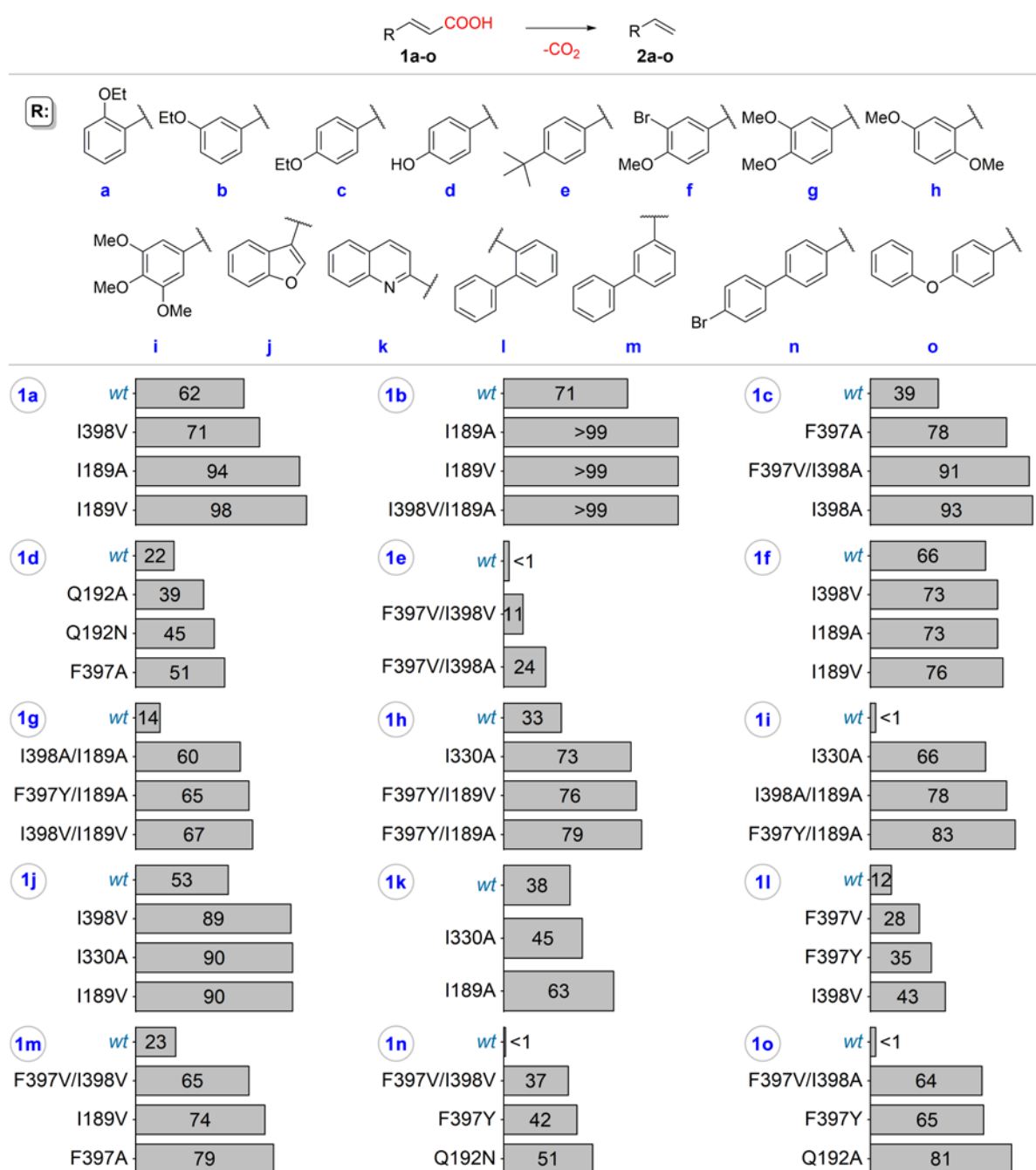


Fig. 3. HPLC conversion values obtained from the analytical scale biotransformation of the substrate panel **1a–1o**, using *ScFDC* whole-cell biocatalyst. Results of the best performing three variants and of the *wild-type ScFDC* are shown.

2.4. Computational studies

Based on previous reports^{1,7,9} and ligand bound *AnFDC* crystal structures (PDB ID: 4ZA7, 4ZA8, 4ZAB), the proper binding of the substrates implies several requirements. Among them, the location of the α - β double bond of the substrate should be in the proximity of the C1' and C4a atoms of the cofactor, necessary for the 1,3-dipolar cycloaddition mechanism (Fig. 1 and Fig. S23). Furthermore, R175 and E285 interact with the carboxyl group of the substrate, while E285 acts also as acid-base in the reaction mechanism, while E280, tunes the pKa of R175 and in turn E285 (Fig. S23)²². Accordingly, the reaction rates are influenced by

multiple substrate-related factors, such as inductive effects of substituents, presence of extended conjugation, substrate orientation related to the prFMN and within the catalytic site, that is influenced by both the size and planarity of the substrate. Considering these factors and using our previously validated molecular docking method⁷, we attempted to gain molecular level insights on the beneficial effect of the mutations on enzyme activities.

Generally, the obtained computational results were in good agreement with the experimentally observed activity enhancements, revealing proper substrate orientations within the catalytic site of the best performing mutant variants. In the following, representative cases are presented, supporting that in contrast to the *wild-type* ScFDC, appropriate mutations relieved the steric hindrance between the substrate and the side chain of the corresponding active site residues. Substrate positioning of representative compounds **1e**, **1i**, **1m**, **1o** within the active site of the corresponding best performing FDC variants is in good agreement with the optimized model of the cinnamic acid bound into the *wild-type* ScFDC1 (Fig. S24).

In the case of *p*-(*tert*-butyl)cinnamic acid **1e**, converted only by variants F397V/I398A and F397V/I398V (Fig. 3), proper binding orientations of **1e** have been obtained within the catalytic site of both variants (Fig. 4a), while within the *wild-type* ScFDC no active substrate-binding state could be observed. The inactivity of the *wt*-ScFDC can be attributed to the steric clash between the *tert*-butyl group of substrate **1e** and the aromatic ring of Phe397, shown in magenta in (Fig. 4a).

In the case of 3,4,5-trimethoxy-cinnamic acid **1i**, the side chains of residues I330 and I189 impede the approach of the substrate to the binding site. The atomic overlap between one of the *meta*-positioned methoxy group of the substrate and the side chain of Ile189 (shown in magenta) can be observed in Fig. 4b, where the optimized model of the of the best performing F397Y/I189A variant is represented.

For bulky substrate **1m**, within the best performing variants, mutation F397A provides space for the biaryl ring system, allowing the proper orientation of the double bond for the 1,3-cycloadditions (Fig. 4c). The mutation relieved the steric hindrance between the two aromatic rings of the F397 side chain and substrate **1m**, which can be noticed in Fig. 4c. It is noteworthy, that this conformation of the substrate corresponds to the ground state geometry, which could explain the improved conversions observed using variant F397A (c=79%) with respect to the *wild-type* enzyme (c=23%).

In case of the similarly bulky substrate **1o**, the etheric group bends the two aromatic rings relatively to each other, resulting in a partial overlap between the *p*-phenoxy substituent group and residue Q192, explaining the enhanced activity of variant Q192A (Fig. 4d) Unfortunately, computational results didn't provide molecular level evidence for the improved activity of variant F397Y.

The strong correlation of the experimental and computational data suggests that the employed molecular model is suitable also for *in-silico* activity predictions for ScFDC, providing a computational tool for the rational engineering of FDC. Notable, that during the preparation of our manuscript *in silico* activity predictions were also reported in tailoring AnFDC and ScFDC for the 1,3-butadiene synthesis³⁶.

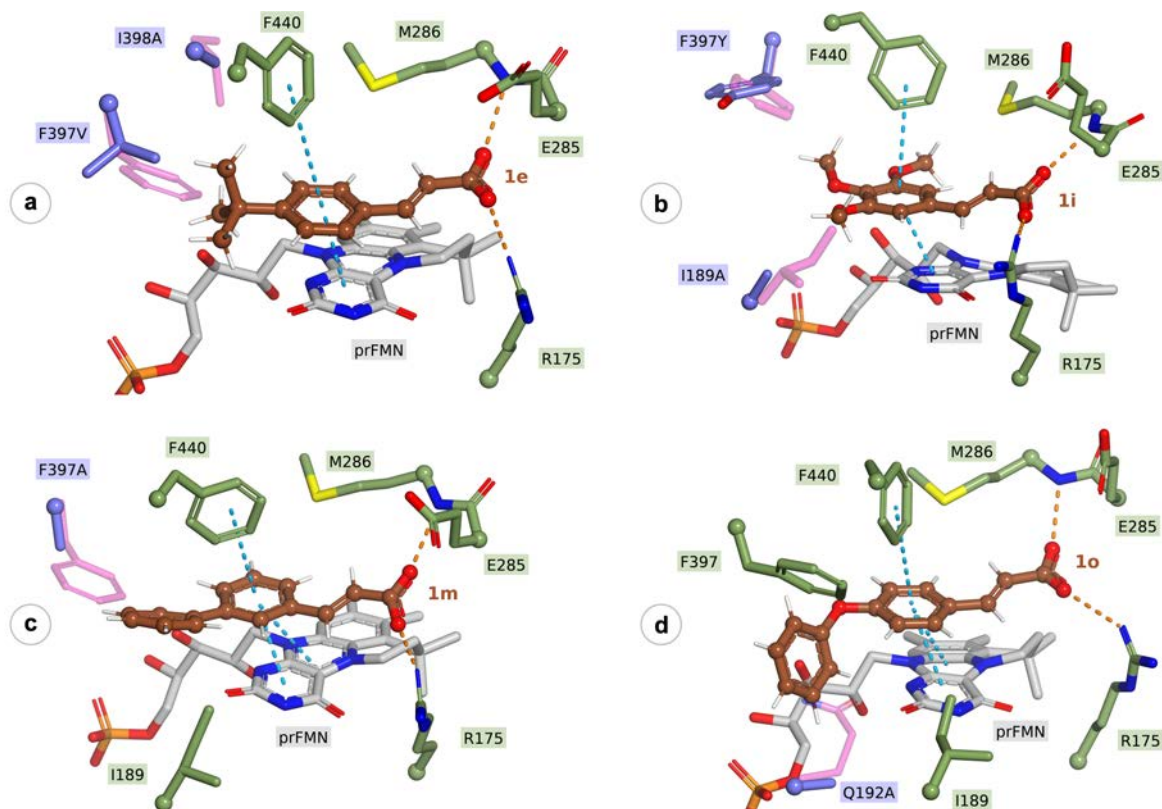


Fig. 4. In each figure the side chains of the preserved active site residues of *ScFDC1* (green) and the mutant residues (blue) overlaid with their original counterparts from the *wild-type* enzyme (magenta) are represented as stick models. The substrates **1e**, **1i**, **1m**, **1o** are colored in brown within Figures **3a**, **3b**, **3c**, **3d**, respectively. Hydrogen bonds between the carboxyl group of the substrate and the backbone nitrogen atom of residue M286 and side chain of residue R175 are indicated as orange dashed lines, whereas the blue dash corresponds to the pi-pi interactions of the substrate's aromatic ring and residue F440 and the prFMN cofactor, respectively. All these interactions were considered within the selection process of the proper binding state, required for the 1,3-cycloaddition mechanism.

3. CONCLUSIONS

Within our study a fluorescent plate assay suitable for the high-throughput (HT) activity screens for ferulic acid decarboxylases (FDCs), has been developed and validated through the activity screens of a mutant library rationally designed towards a 16-membered substrate panel. Identification of mutant variants of enhanced activities provided correlation between the substitution pattern of substrates with their specific active site accommodation. The computational data supported the experimentally observed activity enhancements and revealed proper substrate orientations within the catalytic site of the best performing mutant variants and supported our molecular model for *in silico* FDC-activity predictions. Accordingly, the computational activity predictions, the developed HT-activity assay and the identified substrate specificity modulator residues provide a powerful toolbox for the directed evolution or rational designed based protein engineering of FDCs.

4. EXPERIMENTAL PART

4.1 Materials and methods: see detailed description in *Supporting Information, Chapter 1 and Chapter 2*

4.2 Mutant library generation: the FDC variant library was obtained through site-directed mutagenesis as described in *Supporting information, Chapter 5*.

4.3 Substrate panel generation: the tested substrate library was obtained through the Knoevenagel-Doebner reaction using the corresponding aromatic aldehydes as starting material. For the detailed description of the procedures, obtained yields and NMR data see *Supporting information, Chapter 3*.

4.4. Initial activity screens with cell-plate assay

For all assay plate, whole-cells of *E. coli* Rosetta (DE3) pLysS were used as expression hosts, harboring the pCDF-Duet1 plasmid carrying the genes of *Scfdc1* and *Scpad1* (for detailed description of the plasmid construction, molecular cloning see ESI, Chapter 4.)

2 μ L of cell suspensions harboring the plasmids of each FDC variant were transferred (pipetted) onto LB-agar Petri plates containing chloramphenicol (34.0 μ g/mL), followed by overnight incubation at 37 °C. The colonies grown on the agar plate were transferred on a PVDF membrane, pre-treated by washing with methanol and 100 mM sodium phosphate buffer, pH=7. For successful colony transfer the membrane was left for 20 minutes on the plate. Further, the membrane was transferred to an induction plate (LB-agar with 1 mM IPTG and 34.0 μ g/mL chloramphenicol) and incubated for 8h at 37 °C. Cell permeabilization was performed by placing the membrane under chloroform vapours for 45 second using a desiccator, followed by dialysis on 0.4% agarose plate in 100 mM sodium phosphate buffer, pH=7 and storage at 4 °C, overnight.

The reaction medium plate was prepared by dissolving substrates **1a-p** at 1 mM final concentration in 1% agarose gel, followed by the incubation of the membrane on the reaction plate at 35 °C for 4 hours. For the fluorescent detection of the colonies with FDC activity, the membrane was placed on a filter paper moistened with a solution of 100 M tetrazole in 100 mM sodium phosphate buffer, pH=7 and incubated in dark for 1h at 37 °C, followed by UV-irradiation at 302 nm for 1 min. The detection of signal intensities provided by the colonies of the assay plate was performed by ChemiDoc™ Imaging System, using a corresponding UV filter, allowing detection of specific emissions at >360 nm wavelengths. The obtained images were analyzed by the Image Lab 5.2.1 software, selecting an area of 2.8 mm² from each spot corresponding to the different colonies, for which the background given by the negative control colony has been decreased from the mean values of all pixels inside the boundary volume. The obtained maximum signal intensity value being considered as 100% relative enzyme activity of the other signal intensities provided the corresponding relative activities. All assay-plates have been performed in duplicates, and in all plates the negative controls were represented by the *E. coli* host cells, harbouring the empty pCDF-DUET1 vector.

4.5 Analytical scale biotransformations

4.5.1 Culture preparation

Cultures of *E. coli* BL21(DE3) cells were prepared using Luria-Bertani (LB) medium supplemented with chloramphenicol and streptomycin, that was inoculated with 1-2 v% of overnight culture. Following incubation at 37 °C, 220 rpm, the cultures were induced with IPTG (at a final concentration of 0.2 mM) at OD₆₀₀ ~ 0.6, followed by incubation at 25°C, 220 rpm until to a cell density of OD₆₀₀ ~2. The cells were harvested via centrifugation and immediately used in biotransformations.

4.5.2 Analytical scale FDC mediated decarboxylations

Stock solutions of each substrate in DMSO (50mM) were diluted to 2 mM or to 1 mM in the case of substrates of low solubility, **2k-p**, with phosphate buffer (100 mM NaH₂PO₄, pH 7.0).

The freshly prepared, induced *E. coli* cells harboring *fdc1* genes, were resuspended in the reaction solution to a final OD₆₀₀ of 2, followed by incubation of the reaction mixtures at 35 °C, 700 rpm, for 16 h.

4.5.3. RP-HPLC monitoring

After 16 h of reaction time, the entire reaction mass was subjected to cellular lysis through sonication, followed removing the cellular pellet through centrifugation at 13400 rpm, 12000 g, for 10 min. The cellular pellet was extracted with 500 µL MeOH, which was combined with the supernatant of the previous centrifugation step. 100 µL of the combined solution was diluted with 100 µL of a solution containing 100 mM NaH₂PO₄, pH 7.0, acetonitrile, and benzalacetophenone, used as an internal standard (please refer to *Supporting information, Chapter 7., HPLC methods* for the exact composition of this solution). All HPLC analyses were performed at 25°C using a Phenomenex Kinetex NX-C18 150x4.5 mm column, a mobile phase of 30% H₂O (0,1% v/v TFA) and 70% ACN (0,1% v/v TFA), a flow-rate of 1 mL/min, injecting 5 µL of the previously obtained samples. Conversion values were determined by monitoring the depletion of the substrate concentration, using benzalacetophenone as an internal standard (for detailed description of conversion determination and relative response factors see *Supporting Information, Chapter 7*).

4.6 Molecular docking

The molecular docking calculations were carried out by the Autodock Vina software⁴², using flexible-ligand and rigid-receptor docking. The docking parameters were modified to ensure that among the resulting poses the one with proper binding orientation of the substrate (as defined previously in *Sub-chapter 2.4*) could be identified. Accordingly, a longer search was employed by setting the exhaustiveness of the search to 100, whereas the energy range between the best and worst binding pose was adjusted to 10 kcal/mol. The dimension of the search space was defined by the binding site residues highlighted in Fig. 1 and the prFMN cofactor, based on the crystal structure of ScFDC1 (PDB: 4ZAC)¹, therefore a cubic grid box with the size of 18Å × 18Å × 18Å was employed as it can be seen in Figure S25.

The ground state geometries of the substrates were obtained by means of density functional theory. All quantum chemical calculations were performed by Gaussian 09⁴³ employing the B3LYP density functional with the 6-31G(d,p) basis set, in a water solvated environment using the Polarizable Continuum Model (PCM)⁴⁴.

The crystallographic structure of ScFDC1 was retrieved from Protein Data Bank entry 4ZAC¹. The inactive conformation of residue E285 was altered according to those observed in the ligand bound AnFDC1 crystal structures. The selected docking results were submitted for minimization using the YASARA web server⁴⁵.

ACKNOWLEDGEMENTS

This work was financed by the Swiss National Science Foundation (SNF) project PROMYS, grant no. IZ11Z0_166543. F.A. thanks for the financial support from the Ministry of Research, Innovation and Digitization, CNCS/CCCDI – UEFISCDI, project number PN-III-P1-1.1-PD-2019-1222/PD98 and from project: Entrepreneurship for innovation through doctoral and postdoctoral research, POCU/380/6/13/123886 co-financed by the European Social Fund, through the Operational Program for Human Capital 2014-2020. H.D. thanks the STAR-Institute of the Babeş-Bolyai University for the provided student-research fellowship.

AUTHOR CONTRIBUTIONS

H.D., A.F. contributed to the work equally. H.D. was responsible for the whole-cell biotransformation, including their HPLC-monitoring. A.F. performed the mutant library generation and initial activity screens, using the assay-plate developed together with E.Z.A.N. H.D. and E.Z.A.N. performed the substrate library synthesis, while T.R. was responsible for the spectral analysis of compounds. L.C.N. performed the computational studies and was responsible for the graphical artworks. L.C.B. conceived the project and was responsible for funding together with A.F. L.C.B supervised all experiments, data and wrote the paper together with H.D., A.F., L.C.N. All authors reviewed the manuscript.

ADDITIONAL INFORMATION

Supplementary information to this paper consists of experimental details of molecular cloning, site-directed mutagenesis, synthetic procedures, figures and tables including results of the fluorescent assay plate, tables with HPLC retention times, conversion values for all tested analytical scale biotransformations, and supplementary figures from computational results.

COMPETING INTERESTS STATEMENT. The authors declare no competing interests.

REFERENCES

- 1 Payne, K. A. P. *et al.* New cofactor supports α,β -unsaturated acid decarboxylation via 1,3-dipolar cycloaddition. *Nature* **522**, 497-501, doi:10.1038/nature14560 (2015).
- 2 Ferguson, K. L., Arunrattanamook, N. & Marsh, E. N. G. Mechanism of the Novel Prenylated Flavin-Containing Enzyme Ferulic Acid Decarboxylase Probed by Isotope Effects and Linear Free-Energy Relationships. *Biochemistry* **55**, 2857-2863, doi:10.1021/acs.biochem.6b00170 (2016).
- 3 Ferguson, K. L., Eschweiler, J. D., Ruotolo, B. T. & Marsh, E. N. G. Evidence for a 1,3-Dipolar Cyclo-addition Mechanism in the Decarboxylation of Phenylacrylic Acids Catalyzed by Ferulic Acid Decarboxylase. *Journal of the American Chemical Society* **139**, 10972-10975, doi:10.1021/jacs.7b05060 (2017).
- 4 McKenna, R. & Nielsen, D. R. Styrene biosynthesis from glucose by engineered *E. coli*. *Metabolic Engineering* **13**, 544-554, doi:10.1016/j.ymben.2011.06.005 (2011).
- 5 McKenna, R., Thompson, B., Pugh, S. & Nielsen, D. R. Rational and combinatorial approaches to engineering styrene production by *Saccharomyces cerevisiae*. *Microbial Cell Factories* **13**, doi:10.1186/s12934-014-0123-2 (2014).
- 6 Aleku, G. A. *et al.* Terminal Alkenes from Acrylic Acid Derivatives via Non-Oxidative Enzymatic Decarboxylation by Ferulic Acid Decarboxylases. *ChemCatChem* **10**, 3736-3745, doi:10.1002/cctc.201800643 (2018).
- 7 Nagy, E. Z. A. *et al.* Exploring the substrate scope of ferulic acid decarboxylase (FDC1) from *Saccharomyces cerevisiae*. *Scientific Reports* **9**, doi:10.1038/s41598-018-36977-x (2019).
- 8 Mertens, M. A. S. *et al.* Chemoenzymatic cascade for stilbene production from cinnamic acid catalyzed by ferulic acid decarboxylase and an artificial metatase. *Catalysis Science and Technology* **9**, 5572-5576, doi:10.1039/c9cy01412h (2019).
- 9 Aleku, G. A. *et al.* Enzymatic C–H activation of aromatic compounds through CO₂ fixation. *Nature Chemical Biology* **16**, 1255-1260, doi:10.1038/s41589-020-0603-0 (2020).
- 10 Ogata, T., Yamada, R., Ayuzawa, R. & Nakamura, K. Mutation and Deletion of PAD1 and/or FDC1 and Absence of Phenolic Off-Flavor Production in Top- and Bottom-Fermenting Yeasts. *Journal of the American Society of Brewing Chemists* **78**, 74-79, doi:10.1080/03610470.2019.1678911 (2020).
- 11 Mertens, S. *et al.* Reducing phenolic off-flavors through CRISPR-based gene editing of the FDC1 gene in *Saccharomyces cerevisiae* x *Saccharomyces eubayanus* hybrid lager beer yeasts. *PLoS ONE* **14**, doi:10.1371/journal.pone.0209124 (2019).
- 12 Mukai, N., Masaki, K., Fujii, T. & Iefuji, H. Single nucleotide polymorphisms of PAD1 and FDC1 show a positive relationship with ferulic acid decarboxylation ability among industrial yeasts used in alcoholic beverage production. *Journal of Bioscience and Bioengineering* **118**, 50-55, doi:10.1016/j.jbiosc.2013.12.017 (2014).
- 13 Marshall, S. A. *et al.* in *Methods in Enzymology* Vol. 620 489-508 (2019).
- 14 Richard, P., Viljanen, K. & Penttilä, M. Overexpression of PAD1 and FDC1 results in significant cinnamic acid decarboxylase activity in *Saccharomyces cerevisiae*. *AMB Express* **5**, doi:10.1186/s13568-015-0103-x (2015).
- 15 Grubbe, W. S., Rasor, B. J., Krüger, A., Jewett, M. C. & Karim, A. S. Cell-free styrene biosynthesis at high titers. *Metabolic Engineering* **61**, 89-95, doi:10.1016/j.ymben.2020.05.009 (2020).
- 16 Batyrova, K. A. *et al.* Biocatalytic in Vitro and in Vivo FMN Prenylation and (De)carboxylase Activation. *ACS Chemical Biology* **15**, 1874-1882, doi:10.1021/acscchembio.0c00136 (2020).
- 17 Liu, C. *et al.* A systematic optimization of styrene biosynthesis in *Escherichia coli* BL21(DE3). *Biotechnology for Biofuels* **11**, doi:10.1186/s13068-018-1017-z (2018).
- 18 Mukai, N., Masaki, K., Fujii, T., Kawamukai, M. & Iefuji, H. PAD1 and FDC1 are essential for the decarboxylation of phenylacrylic acids in *Saccharomyces cerevisiae*. *Journal of Bioscience and Bioengineering* **109**, 564-569, doi:10.1016/j.jbiosc.2009.11.011 (2010).

- 19 Gulmezian, M., Hyman, K. R., Marbois, B. N., Clarke, C. F. & Javor, G. T. The role of UbiX in Escherichia coli coenzyme Q biosynthesis. *Archives of Biochemistry and Biophysics* **467**, 144-153, doi:10.1016/j.abb.2007.08.009 (2007).
- 20 Lin, F., Ferguson, K. L., Boyer, D. R., Lin, X. N. & Marsh, E. N. G. Isofunctional enzymes PAD1 and UbiX catalyze formation of a novel cofactor required by ferulic acid decarboxylase and 4-hydroxy-3-polyprenylbenzoic acid decarboxylase. *ACS Chemical Biology* **10**, 1137-1144, doi:10.1021/cb5008103 (2015).
- 21 Balaikaite, A. *et al.* Ferulic Acid Decarboxylase Controls Oxidative Maturation of the Prenylated Flavin Mononucleotide Cofactor. *ACS Chemical Biology* **15**, 2466-2475, doi:10.1021/acscchembio.0c00456 (2020).
- 22 Bailey, S. S. *et al.* The role of conserved residues in Fdc decarboxylase in prenylated flavin mononucleotide oxidative maturation, cofactor isomerization, and catalysis. *Journal of Biological Chemistry* **293**, 2272-2287, doi:10.1074/jbc.RA117.000881 (2018).
- 23 Khusnutdinova, A. N. *et al.* in *Methods in Enzymology* Vol. 620 469-488 (2019).
- 24 Wang, P. H. *et al.* Biosynthesis and Activity of Prenylated FMN Cofactors. *Cell Chemical Biology* **25**, 560-570.e566, doi:10.1016/j.chembiol.2018.02.007 (2018).
- 25 Annaival, T. *et al.* Biochemical and Structural Characterization of TtnD, a Prenylated FMN-Dependent Decarboxylase from the Tautomycin Biosynthetic Pathway. *ACS Chemical Biology* **13**, 2728-2738, doi:10.1021/acscchembio.8b00673 (2018).
- 26 Mergelsberg, M. *et al.* Phthaloyl-coenzyme A decarboxylase from *Thauera chlorobenzoica*: the prenylated flavin-, K⁺- and Fe²⁺-dependent key enzyme of anaerobic phthalate degradation. *Environmental Microbiology* **19**, 3734-3744, doi:10.1111/1462-2920.13875 (2017).
- 27 Payer, S. E. *et al.* Regioselective para-Carboxylation of Catechols with a Prenylated Flavin Dependent Decarboxylase. *Angewandte Chemie - International Edition* **56**, 13893-13897, doi:10.1002/anie.201708091 (2017).
- 28 Payne, K. A. P. *et al.* Structure and Mechanism of *Pseudomonas aeruginosa* PA0254/HudA, a prFMN-Dependent Pyrrole-2-carboxylic Acid Decarboxylase Linked to Virulence. *ACS Catalysis* **11**, 2865-2878, doi:10.1021/acscatal.0c05042 (2021).
- 29 Gu, W. *et al.* Structural basis of enzymatic activity for the ferulic acid decarboxylase (FADase) from *Enterobacter* sp. Px6-4. *PLoS ONE* **6**, doi:10.1371/journal.pone.0016262 (2011).
- 30 Wuensch, C. *et al.* Asymmetric enzymatic hydration of hydroxystyrene derivatives. *Angewandte Chemie - International Edition* **52**, 2293-2297, doi:10.1002/anie.201207916 (2013).
- 31 Payer, S. E. *et al.* Exploring the Catalytic Promiscuity of Phenolic Acid Decarboxylases: Asymmetric, 1,6-Conjugate Addition of Nucleophiles Across 4-Hydroxystyrene. *Advanced Synthesis and Catalysis* **359**, 2066-2075, doi:10.1002/adsc.201700247 (2017).
- 32 Zhang, X. *et al.* Biochemical characterization and substrate profiling of a reversible 2,3-dihydroxybenzoic acid decarboxylase for biocatalytic Kolbe-Schmitt reaction. *Enzyme and Microbial Technology* **113**, 37-43, doi:10.1016/j.enzmictec.2018.02.008 (2018).
- 33 Bhuiya, M. W., Lee, S. G., Jez, J. M. & Yu, O. Structure and mechanism of ferulic acid decarboxylase (FDC1) from *Saccharomyces cerevisiae*. *Applied and Environmental Microbiology* **81**, 4216-4223, doi:10.1128/AEM.00762-15 (2015).
- 34 Lan, C. L. & Chen, S. L. The Decarboxylation of α,β -Unsaturated Acid Catalyzed by Prenylated FMN-Dependent Ferulic Acid Decarboxylase and the Enzyme Inhibition. *Journal of Organic Chemistry* **81**, 9289-9295, doi:10.1021/acs.joc.6b01872 (2016).
- 35 Tian, G. & Liu, Y. Mechanistic insights into the catalytic reaction of ferulic acid decarboxylase from *Aspergillus niger*: A QM/MM study. *Physical Chemistry Chemical Physics* **19**, 7733-7742, doi:10.1039/c6cp08811b (2017).
- 36 Mori, Y., Noda, S., Shirai, T. & Kondo, A. Direct 1,3-butadiene biosynthesis in *Escherichia coli* via a tailored ferulic acid decarboxylase mutant. *Nature Communications* **12**, doi:10.1038/s41467-021-22504-6 (2021).
- 37 Moisă, M. E. *et al.* Fluorescent enzyme-coupled activity assay for phenylalanine ammonia-lyases. *Scientific Reports* **10**, doi:10.1038/s41598-020-75474-y (2020).

- 38 Lee, Z. Y., Raghavan, S. S., Ghadessy, F. J. & Teo, Y. N. Rapid and sensitive detection of acrylic acid using a novel fluorescence assay. *RSC Advances* **4**, 60216-60220, doi:10.1039/c4ra12495b (2014).
- 39 Shang, X. *et al.* Improved Photoinduced Fluorogenic Alkene-Tetrazole Reaction for Protein Labeling. *Bioconjugate Chemistry* **28**, 2859-2864, doi:10.1021/acs.bioconjchem.7b00562 (2017).
- 40 Wang, Y., Song, W., Hu, W. J. & Lin, Q. Fast alkene functionalization in vivo by photoclick chemistry: HOMO lifting of nitrile imine dipoles. *Angewandte Chemie - International Edition* **48**, 5330-5333, doi:10.1002/anie.200901220 (2009).
- 41 An, P., Lewandowski, T. M., Erbay, T. G., Liu, P. & Lin, Q. Sterically Shielded, Stabilized Nitrile Imine for Rapid Bioorthogonal Protein Labeling in Live Cells. *Journal of the American Chemical Society* **140**, 4860-4868, doi:10.1021/jacs.8b00126 (2018).
- 42 Trott, O. & Olson, A. J. AutoDock Vina: Improving the speed and accuracy of docking with a new scoring function, efficient optimization, and multithreading. *Journal of Computational Chemistry* **31**, 455-461 (2010).
- 43 Gaussian 09 (Revision E.01) (Gaussian Inc., Wallingford CT, 2009).
- 44 Tomasi, J., Mennucci, B. & Cammi, R. Quantum mechanical continuum solvation models. *Chemical Reviews* **105**, 2999-3093, doi:10.1021/cr9904009 (2005).
- 45 Krieger, E. *et al.* Improving physical realism, stereochemistry, and side-chain accuracy in homology modeling: Four approaches that performed well in CASP8. *Proteins: Structure, Function and Bioinformatics* **77**, 114-122, doi:10.1002/prot.22570 (2009).